

# Development and Characterization of a Non-Intrusive Magnetic Sensor to Measure Wear in Centrifugal Pumps

Bryan Bohn, Ramin Khoie, Bhushan Gopaluni, *Member, IEEE*, James A. Olson, and Boris Stoeber, *Senior Member, IEEE*

**Abstract**—A magnetic sensor is designed and fabricated that allows for impeller blade wear measurement while a centrifugal pump is in operation. The sensor can be installed on existing pumps and does not require structural modification. Over time, as the pump impeller erodes, the gap between the impeller and pump side plate increases from an unworn width of 0.65 mm to 2.50 mm, the maximum allowable wear on the testbed pump used for experimental validation. The extent of the impeller wear is determined by measuring over time the change in reluctance of a magnetic circuit passing through the eroding area. The sensor flux guide mechanism has a relative magnetic permeability of 10,000. Flux through the circuit is driven by an inductive coil excited with a 1.0 V AC voltage signal at 70 Hz. As wear occurs, the impeller gap grows and the total reluctance of the magnetic circuit increases, which cause the peak inductance of the coil to drop. Trial data is collected at a sampling frequencies up to 500 kHz and then assessed in the frequency domain using Fast Fourier transform (FFT). The amplitude of the FFT signal at the pump's rotational frequency is then considered to estimate wear. Sampling data for one second at 500 kHz, the sensor demonstrates a maximum signal to noise ratio of 17.8 dB with an average sensitivity of 0.022 mV/mm and resolution of 0.38 mm.

**Index Terms**—Magnetic Sensor, Wear Detection, Centrifugal Pumps, Reluctance Sensor

## INTRODUCTION

CENTRIFUGAL pumps account for between 25% and 60% of the total electrical motor energy consumed in processing plants of various industries [1]. After prolonged periods of use, erosion inside centrifugal pumps causes a reduction in pumping efficiency and may ultimately lead to wasted electrical power or outright failure [2]. In open-impeller centrifugal pumps, mechanical wear is usually most prevalent on the tips of the pump's impeller blades (Fig. 1) [3]. Over time, this erosion increases the gap between the pump's impeller and side plate, giving rise to undesirable behaviors like recirculating flow and cavitation.

Erosion in centrifugal pumps can be caused by a variety of physical and process factors. Typically, the phenomenon is a cumulative consequence of abrasion, cavitation, and oxidation. Presently, there are no widely practicable methods for directly

measuring physical erosion inside industrial centrifugal pumps while the pump is operating.



Fig. 1. A two-blade centrifugal pump impeller used for moving a slurry of water and paper pulp. Erosion often manifests in the region denoted in orange.

Mechanical surface wear can be measured through a variety of techniques. A previous study by F. Schmaljohann et al. has assessed the magnitude of wear on metallic surfaces through the deposition of a thin resistive film [4]. As wear occurs, the resistance of the film increases, which can be correlated to identify the magnitude of the erosion. The concept is successfully applied to measure wear on the surface of a machining tool. It is, however, unsuitable for the mutable, aqueous environment of a centrifugal pump. In addition, the deposition of a thin resistive film on the working surface requires specialized tools and disruption of operation, increasing the cost and inconvenience of implementation.

G. Rutelli et al. demonstrate a camera-based wear sensor for a lathe machine application [5]. The captured images are post-processed to characterize wear with an accuracy of 0.010 mm. However, the method requires visual access to the wearing surface, which is not readily achievable in the context of an operating centrifugal pump. Therefore, surface wear measurement on an impeller is not practical with this approach.

N. Ghosh et al. propose a more multifaceted approach for capturing the dynamics of wear during a CNC milling process [6]. This work demonstrates a concept for a neural-network-based sensor system that measures cutting forces, vibration, spindle current, sound, and pressure during a milling process

This research is supported by the Energy Reduction in Mechanical Pulping (ERMP) program at The University of British Columbia. Supporting partners of the ERMP program are: Alberta Newsprint Company, AB Enzymes, Andritz, BC Hydro, Canfor Pulp, Catalyst Paper, FPInnovations, Holmen, Meadow Lake Pulp, Millar Western, NORPAC, NSERC, Westcan Engineering, and Winstone Pulp International. This research was undertaken, in part, thanks to funding from the Canada Research Chairs program. An earlier version of this

paper was presented at the IEEE Sensors Conference 2015 and was published in its Proceedings (<https://ieeexplore.ieee.org/document/7370367>) [10].

B. Bohn, B. Gopaluni, J. Olson, and B. Stoeber are with The University of British Columbia, Vancouver, BC, Canada (email: bryan.bohn@ubc.ca). Ramin Khoie was with The University of British Columbia. He is now with AutomationX, Vancouver, BC, Canada (email: ramin@rkhoie.com).

with the intent of classifying cutting tool surface degradation. While the study demonstrates a potential avenue for characterizing the broader behavior and mechanisms of impeller wear, the system complexity and corresponding cost would make it unworkable for use in typical industrial pumping applications.

The research herein demonstrates a standalone, portable, externally-mounted magnetic sensor that detects surface wear on a centrifugal pump impeller while the pump is operating. Whereas other wear measurement methods require physical alteration (either through the addition of resistive coatings, permanent installation of sensors, etc.) and disruptions to normal operation, the described sensor requires no structural or process modifications to the target system. As a result, this sensor has reduced implementation costs and complexity, making it a more viable option for pumping applications where the benefits of minimizing waste energy and process interruptions must be weighed against the practical costs of employing a wear-monitoring system in the first place.

The testbed system used throughout this research is a two-blade, open-impeller, 40-horsepower centrifugal pump manufactured by Westcan Industries Ltd., Canada. The adjoining fluid system is part of the Pulp and Paper Centre Pilot Plant at The University of British Columbia in Vancouver, BC, Canada.

#### SENSOR PRINCIPLE

The conceived sensor uses a magnetic circuit to measure wear inside a centrifugal pump. The centrifugal pump is placed in the path of the circuit, the bulk of which is made from high-permeability material to guide the flux and minimize flux leakage. The circuit directs flux through the pump housing, side plate, impeller, and stuffing box. Between the side plate and impeller is a fluid-filled gap that increases with wear. This gap, highlighted in Fig. 2, is the point of measurement interest.

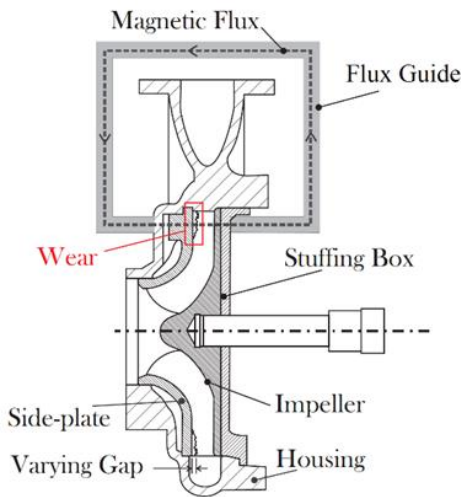


Fig. 2. A concept for using a magnetic sensor to observe wear on the surface of a centrifugal pump impeller.

The magnitude of the flux carried inside the circuit is derived from two of Maxwell's equations [8]. According to Ampère's

Law,

$$\oint \vec{H} \cdot d\vec{l} = \int J \cdot d\vec{A} = i, \quad (1)$$

where the closed line integral of the magnetic field  $\vec{H}$  over the length of the magnetic circuit  $l$  equals the current density  $J$  through the area  $A$  and the total free electrical current  $i$ . For an inductive coil, the line integral of the magnetic field strength, as represented in (1), is

$$\sum H \cdot \Delta l = N \cdot i_{coil}, \quad (2)$$

where  $i_{coil}$  represents electrical current passing through  $N$  coil windings. Here, the coil would be wrapped around the flux guide. Gauss' law,

$$\oint \vec{B} \cdot d\vec{A} = 0, \quad (3)$$

states that the integral of the magnetic flux density  $\vec{B}$  over the surface area  $A$  of any enclosed volume is zero. The magnetic field inside the circuit and the flux density are related through the magnetic permeability  $\mu$  such that

$$\vec{B} = \mu \vec{H}, \quad (4)$$

where

$$\mu = \mu_0 \mu_r, \quad (5)$$

with the relative permeability of the medium  $\mu_r$  and the magnetic permeability of free space  $\mu_0 = 4\pi \cdot 10^{-7} H/m$ .

The centrifugal pump considered in this study is used to transport water and suspensions of water with low-concentration paper pulp. The relative magnetic permeabilities of water and wood pulp are approximately that of the air ( $\mu_{r,water} \cong \mu_{r,wood} \cong \mu_{r,air} \cong 1$ ), therefore the gap inside the wearing pump can be suitably approximated as a free space gap. Solving (1) through (5), the magnetic flux density through the guide can be written as a function of the flux guide parameters; relative permeability  $\mu_c$ , cross-sectional area  $A_c$ , and length  $l_c$ , and the parameters of the gap; relative permeability  $\mu_r \sim 1$ , cross-sectional area  $A_{gap}$  and length  $l_{gap}$ .

$$B = \frac{N}{\frac{l_{gap}}{\mu_0 \mu_r A_{gap}} + \frac{l_c}{\mu_0 \mu_c A_c}} i_{coil} \quad (6)$$

Equation (6) similarly depends on the number of coil windings  $N$ , cross-sectional area of the coil  $A_{coil}$ , and current  $i_{coil}$ . It can be observed that the generated flux density  $B$  is inversely proportional to the width of the air gap  $l_{gap}$ . Equation (6) can be written in terms of the magnetic reluctance

$$\mathfrak{R} = \frac{l}{\mu A}, \quad (7)$$

which is a function of geometry and material properties for each element inside the circuit. Simplifying Equation (6) with

Equation (7) yields the magnetic flux density

$$B = \frac{\frac{N}{A_{coil}}}{\mathfrak{R}_{gap} + \mathfrak{R}_{fluxguide}} i_{coil}, \quad (8)$$

where the gap in the circuit increases its corresponding reluctance  $\mathfrak{R}_{gap}$ .

A schematic of a circuit model that more closely describes the geometry and material properties of the pump parts in the circuit is shown in Fig. 3.

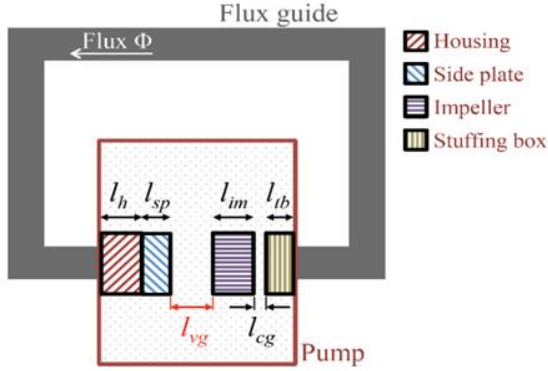


Fig. 3. Conceptual diagram of the magnetic sensor passing flux through components of a centrifugal pump. The variable gap  $l_{vg}$  is highlighted in red.

To measure the width of the varying gap  $l_{vg}$ , the total change in reluctance of the circuit is determined. The total reluctance

$$\mathfrak{R}_{total} = \mathfrak{R}_{vg} + \mathfrak{R}_{static} \quad (9)$$

comprises the variable reluctance caused by the varying impeller gap

$$\mathfrak{R}_{vg} = \frac{l_{vg}}{\mu_o A_{vg}} \quad (10)$$

and the static reluctance

$$\mathfrak{R}_{static} = \frac{l_h}{\mu_o \mu_p A_h} + \frac{l_{sp}}{\mu_o \mu_p A_{sp}} + \frac{l_{im}}{\mu_o \mu_p A_{im}} + \frac{l_{cg}}{\mu_o A_{cg}} + \frac{l_{tb}}{\mu_o \mu_p A_{tb}} + \frac{l_c}{\mu_o \mu_c A_c} \quad (11)$$

of the remaining pump components, as detailed in Table I. The effective area of each component in the magnetic circuit is estimated through flux simulations. As wear occurs at the tip of the impeller blades, the magnitude of the varying reluctance is increased, which yields an increase in the total reluctance of the circuit.

This reluctance can be monitored by measuring the inductance of the coil around the flux guide. The inductance of a coil is a function of its core's reluctance value. Integrated with the flux guide assembly, the inductance of the coil

$$L_{coil} = \frac{N^2}{\mathfrak{R}_{total}} \quad (12)$$

can be written as a function of the number of coil windings  $N$ , and the total reluctance of the magnetic circuit from (9). This suggests that as the reluctance of the circuit increases due to wear, the inductance of the magnetic coil decreases. This behavior forms an operating basis for monitoring wear while the pump is in operation. Combining (9) through (12), the inductance of the coil,

$$L_{coil} = \frac{N^2}{\frac{l_{vg}}{\mu_o A_{vg}} + \mathfrak{R}_{static}}, \quad (13)$$

can be written as a function of the variable gap width  $l_{vg}$ .

Solving analytically using the flux path parameters in Table I and a 150-turn coil yields the change in the inductance of the magnetic coil as the gap width increases from the unworn state of 0.65 mm to maximum allowable wear gap of 2.50 mm. The analytical response is shown in Fig. 4. It is observed that the inductance decreases from 15.1 mH to 7.6 mH as a result of the increasing gap.

TABLE I  
MAGNETIC FLUX PATH PARAMETERS

Element	Symbols	Length $l$ [mm]	Effective Area $A$ [mm <sup>2</sup> ]	Relative permeability $\mu_r$
Variable gap	$l_{vg}, A_{vg}$	0.65-2.50	1000	1
Housing	$l_h, A_h$	10	$10^4$	500
Stuffing box	$l_{tb}, A_{tb}$	15	$10^4$	500
Constant gap	$l_{cg}, A_{cg}$	10	$10^4$	1
Side plate	$l_{sp}, A_{sp}$	11	$10^4$	500
Impeller	$l_{im}, A_{im}$	38	400	500
Flux guide	$l_c, A_c$	640	2000	$10^4$

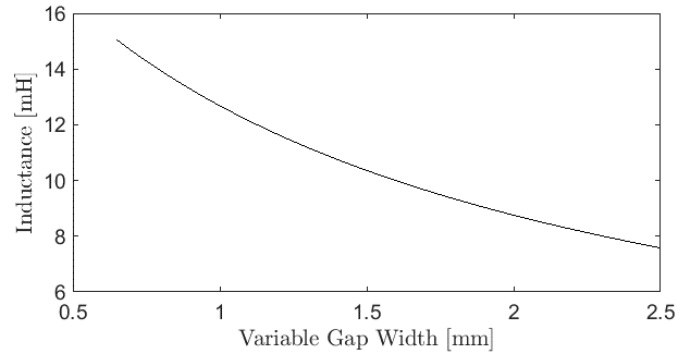


Fig. 4. Analytical model of coil inductance as a function of impeller gap.

Electrical noise is typically high in an industrial pumping environment. Since an AC voltage signal is used to operate the magnetic coil at a fixed frequency, the output signal can be collected at the excitation frequency to reduce the effect of any DC or AC noise apparent in the environment.

The variable-reluctance inductance approach appears suitable for determining the extent of impeller wear. A slightly different approach is also explored [7], where the magnetic flux in the flux guide would be measured. The magnetic flux could be provided by a coil or a permanent magnet and would vary with impeller wear. However, measuring the magnetic flux with a Hall effect sensor requires an additional air gap in the

flux guide, which increases the static reluctance of the magnetic circuit and causes a significant decrease in sensitivity. In addition, magnetic field noise from nearby permanent magnets has the potential to impact the behavior of the Hall effect sensor more significantly than the wearing impeller itself. Further, the presence of the Hall effect sensor contributes to the complexity of the physical fabrication of the flux guide sensor. An inductive coil is therefore most practical for the described application, based on measurement sensitivity, signal-to-noise ratio, and device complexity.

## SENSOR DESIGN

The physical parameters of the flux guide are fundamental to the sensor's behavior. The principal design factors are the material properties and the physical geometry.

### A. Flux Guide Material

Magnetic permeability, cost, and saturation flux density dictate a material's suitability for use as a flux guide. To identify the magnetic permeability required for the flux guide assembly, the effect of permeability on the output of the sensor is evaluated using the analytical model in (13), as shown in Fig. 5.

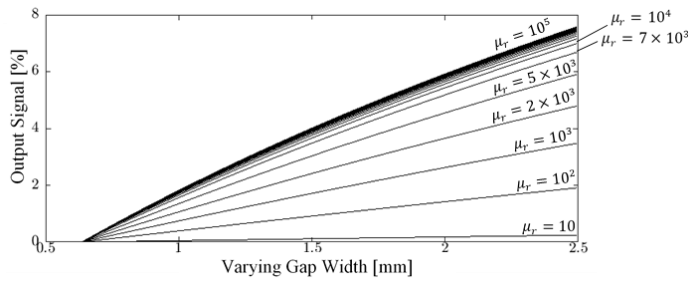


Fig. 5. Percentage change in sensor output signal (coil inductance) as a function of impeller gap width for relative magnetic permeabilities between 10 and  $10^5$ .

As the magnetic permeability of the flux guide material increases, the sensitivity of the sensor improves, reaching diminishing gains beyond  $\mu_r = 10^4$ . This suggests that there is little practical benefit to utilizing materials with permeability exceeding this limit. In Table II, several alternatives are considered and compared based on their magnetic permeability, saturation flux density, and cost.

TABLE II  
PROPERTIES OF HIGH-MAGNETIC-PERMEABILITY MATERIALS CONSIDERED FOR FLUX GUIDE

Material	Relative Permeability <sup>1</sup>	Saturation Flux Density	Cost Per Mass <sup>2</sup>
M100	$10^4$	0.42 T	\$67/kg
VimVar	$10^4$	2.15 T	\$65/kg
Hiperco 50	$1.5 \times 10^4$	2.42 T	\$251/kg
Hy-Mu 80	$23 \times 10^4$	0.87 T	\$81/kg

<sup>1</sup> Relative permeability refers to the maximum permeability achievable from the material.

<sup>2</sup> The materials in this table have comparable densities. The total weight of the flux guide assembly is approximately 20 kg.

M100 and VimVar are suitable options for the fabrication of the flux guide assembly. However, M100 has equivalent initial and peak permeability (i.e. it does not require a bias field to reach the stated peak permeability), whereas VimVar does not. This simplifies the sensor fabrication and instrumentation, thus, M100 is the optimal choice. M100 is a brand name for a Manganese Zinc Iron Ferrite alloy manufactured by National Magnetics Group Incorporation in the United States.

### B. Sensor Geometry

As the flux guide assembly constitutes the main body of the sensor, it is designed to be easy to fabricate, affordable, and robust, with maximized sensitivity. It contains an adjustable clamping mechanism to allow for reliable attachment to the exterior of a variety of centrifugal pumps. M100 is a brittle material and not conventionally machinable, so the flux guide geometry minimizes required machining. Several iterations of clamping mechanisms lead to the final 'C'-shaped geometry presented in Fig. 6.

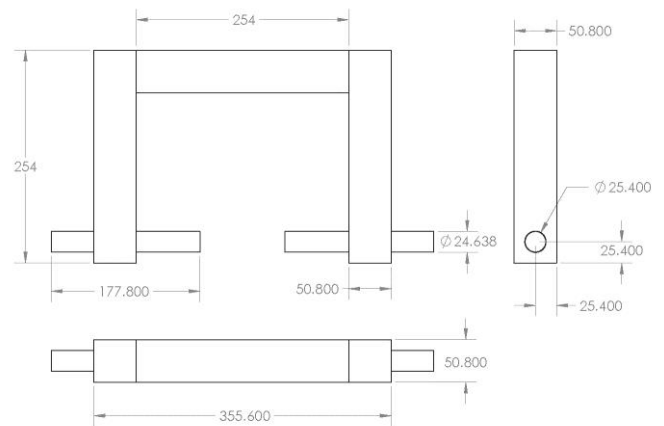


Fig. 6. The flux guide assembly geometry. All dimensions are in mm.

### C. Coil Design

Through optimization simulations it is determined that the number of turns on the coil does not have a significant impact on overall sensitivity as long as flux saturation is avoided. A single-layer coil with 150 turns is selected for the prototype sensor. To ensure that the inductor is capable of carrying the requisite current, the coil is constructed to safely operate up to 100 mA at 200 kHz. Based on these parameters, an American Wire Gage (AWG) 30 wire with enamel coating is selected for the coil.

The parasitic capacitance  $C_{par}$  for a single layer inductor is defined as

$$C_{par} \cong 1.366C_u \quad (14)$$

The turn-to-turn capacitance  $C_u$  is determined by the permittivity and other physical parameters of the inductor wire. The estimated parasitic capacitance of the coil is 26.3 pF [9] leading to a self-resonance of the coil around 100 kHz. The coil resistance is approximately 10.3  $\Omega$ . The parasitic capacitance between coil windings is considered sufficiently small and can be neglected.

#### D. Simulation

A model of the pump and sensor is developed using Comsol Multiphysics. The model includes all the components of the pump to scale, with exception to the impeller, which is approximated as a straight vane to simplify the geometry. The simulated pump is shown in Fig. 7.

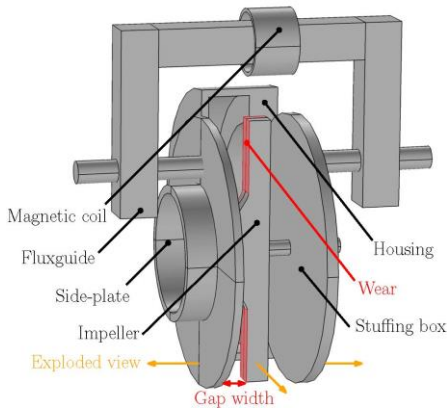


Fig. 7. A cutaway view of the sensor and centrifugal pump model.

The modelled impeller is static for each simulation, however the angular position of the impeller can be manipulated to achieve an angle-dependent response. For each simulation, the magnetic coil excitation frequency and current are 100 Hz and 10 mA, respectively. The simulated flux guide and pump components have the magnetic properties of M100 and cast iron, respectively.

While the square flux guide is practical to fabricate, sharp corners have a tendency to amplify the magnitude of magnetic flux and cause saturation. A flux density evaluation is performed to verify suitable flux capacity through the flux guide. The saturation flux density of the M100 material is 420 mT, while the simulation yields a maximum local flux density 5 mT and negligible flux leakage. The non-linear effects of flux saturation are therefore negligible. In addition, the simulation shows a negligible amount of flux passing through the pump housing, avoiding the impeller.

The coil serves the dual purpose of generating magnetic flux and establishing the total reluctance of the magnetic circuit. The inductance response to changing impeller position, as simulated with Comsol Multiphysics, is shown in Fig. 8. The peaks at  $0^\circ$ ,  $180^\circ$ , and  $360^\circ$  correspond to an impeller blade passing through the flux path.

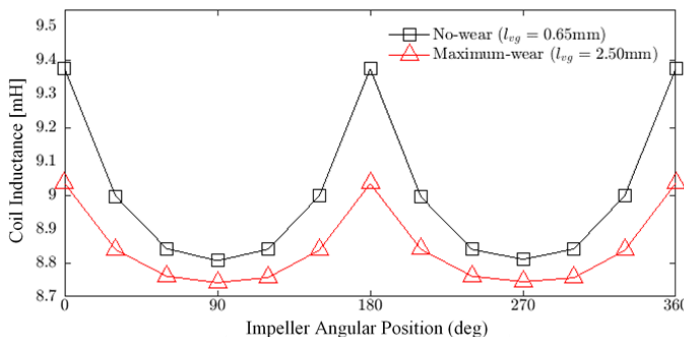


Fig. 8. Simulated coil inductance versus impeller position at a current of 10 mA and frequency of 100 Hz.

Fig. 8 demonstrates that the inductance maxima at  $0^\circ$ ,  $180^\circ$ , etc. decrease from wear. The simulation in Fig. 9 shows the decreasing trend of those maxima as the impeller wears and the gap grows.

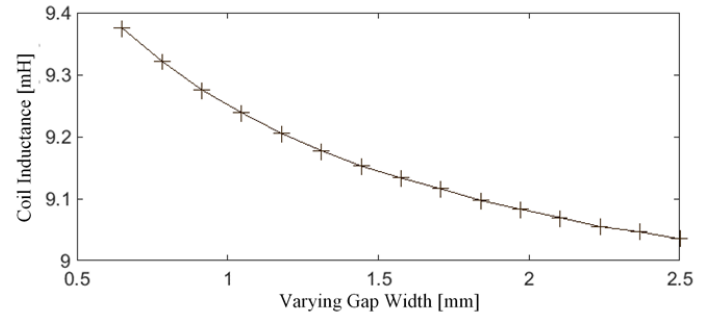


Fig. 9. Simulated coil inductance as a function of varying impeller gap at a current of 10 mA and frequency of 100 Hz.

#### INSTRUMENTATION

Auxiliary instrumentation and circuitry are required to operate the magnetic sensor. The external circuitry comprises electronics for driving the inductive coil and performing inductance measurements. The sensor measurement circuit is shown in Fig. 10.

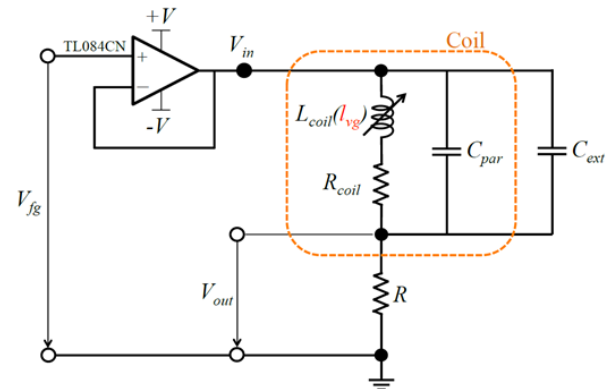


Fig. 10. The measurement circuit, including the voltage follower circuit.

An external capacitor with capacitance  $C_{ext}$  is connected in parallel with the coil. Combined with the parasitic capacitance of the coil  $C_{par}$ , this creates a total capacitance

$$C = C_{ext} + C_{par}, \quad (15)$$

that results in a reduced resonant frequency compared to the self-resonance of the coil. Driving the circuit near resonance leads to high sensitivity, as small changes in the coil inductance cause large changes in the impedance of the coil and the parallel external capacitor. To measure the inductance, a shunt resistor with resistance  $R$  is connected in series with the coil and the capacitor, and a voltage  $V_{in}$  is applied across the entire circuit. The output voltage across the shunt resistor is a measure for the inductance of the magnetic coil inside the sensor. The inductance value is then used to estimate wear on impeller blades of the centrifugal pump.

The ratio between the output voltage over the input voltage is calculated by

$$\left| \frac{V_{out}}{V_{in}} \right| = \sqrt{\frac{[R(1-\omega^2 L_{coil} C)]^2 + \omega^2 R^2 R_{coil}^2 C^2}{(R_{coil} + R - \omega^2 R L_{coil} C)^2 + (\omega L + \omega R R_{coil} C)^2}}, \quad (16)$$

with the angular frequency  $\omega = 2\pi f$ , a function of the excitation frequency  $f$ .

Simulations suggest that to minimize the effect of eddy currents the excitation frequency is best chosen below 100 Hz. The external capacitance  $C_{ext} = 100 \mu F$  is selected to achieve a resonant frequency around 100 Hz. An optimization based on (16) yields a maximum sensitivity when  $R = 7.5 \Omega$ . Similarly, optimizing (16) using the selected circuit component properties yields a maximum sensitivity for the excitation frequency  $f = 70 \text{ Hz}$ .

### EXPERIMENTAL VALIDATION

The hardware setup for empirical validation of the prototype device consists of the sensor and driving coil assembly, inductance measurement circuit, a National Instruments NI USB-6212 data acquisition hub, and a laptop operating National Instruments LabView software. The prototype sensor is shown in Fig. 11, mounted to a centrifugal pump.

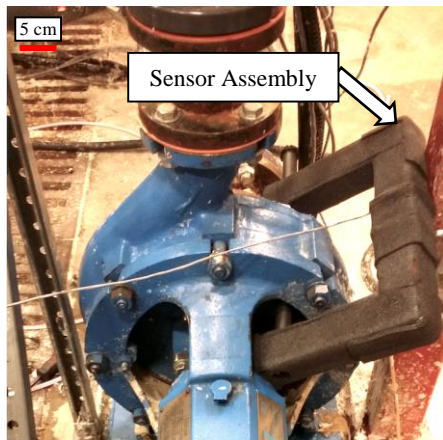


Fig. 11. The prototype magnetic sensor mounted to the testbed pump.

To measure the inductance  $L_{coil}$  from the frequency response of the sensor, only the lower frequency readings of the output signal are considered, where the effect of the parasitic capacitance of the coil can be neglected. Assuming no parasitic capacitance, the magnitude of the output voltage over the input voltage

$$\left| \frac{V_{out}}{V_{in}} \right| = \frac{R + R_{coil}}{\sqrt{(R + R_{coil})^2 + (2\pi f L_{coil})^2}} \quad (17)$$

is written merely as a function of the known resistance  $R + R_{coil}$  and the coil's inductance. Solving for

$$L_{coil} = \frac{R}{2\pi f} \sqrt{\left( \frac{V_{in}}{V_{out}} \right)^2 - 1} \quad (18)$$

and applying a least squares estimation, the inductance of the magnetic coil is estimated to be 33.1 mH, which is within the same order of magnitude as the inductance value predicted from the simulated results for the pump-mounted sensor. The greater inductance value observed in the physical measurement is due to the circuit being fully closed, with the sensor probes in contact with each other, whereas the simulated model includes the pump components and variable gap.

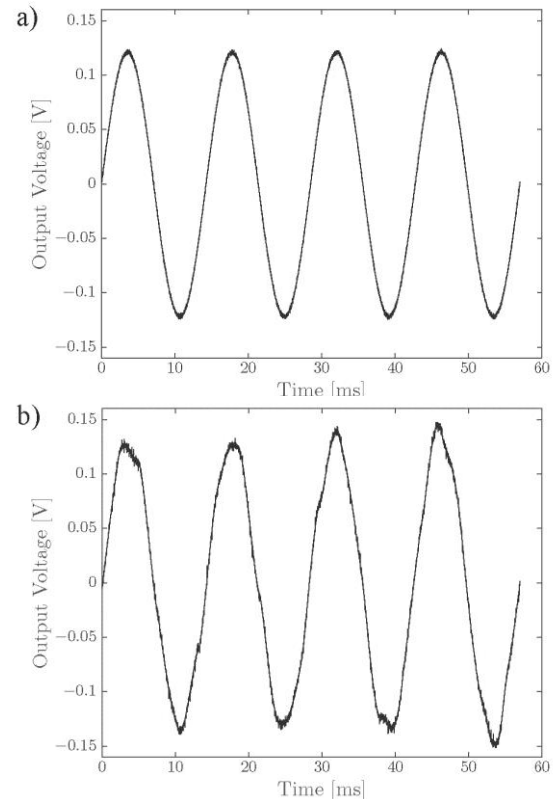
The resonant frequency of the coil

$$f_{res} = \frac{1}{2\pi\sqrt{L_{coil}C_{par}}}, \quad (19)$$

is around 160 kHz. Using (19), the parasitic capacitance of the coil is calculated to be 29.8 pF – close to the analytical prediction of 26.3 pF. It is easily verified that neglecting the parasitic capacitance when determining the inductance is justified.

### RESULTS AND ANALYSIS

After installing the sensor on the testbed centrifugal pump, data is collected while the pump is stationary to analyze the voltage signal output. During the measurements, the coil is excited at 70 Hz and data is collected at a sampling frequency of 50 kHz for a duration of one second. The rotational speed of the pump is then increased to 900 RPM using a Variable Frequency Drive (VFD). Data is again collected with the same sampling conditions and the output of the sensor is plotted in the time domain. The time-domain output signals for both



states are shown in Fig. 12.

Fig. 12. The output voltage signal from the sensor as a function of time for a) the static pump, and b) the pump rotating at 900 RPM.

To analyze the change in the behavior of the circuit as a function of impeller wear inside the pump, the time domain signal  $V_{out}(t)$  is then transformed to the frequency domain equivalent  $V_{out}(f)$  using the Fast Fourier Transform (FFT) algorithm. The resulting plot of the sensor's output signal at a pump operating speed of 900 RPM is shown in Fig. 13.

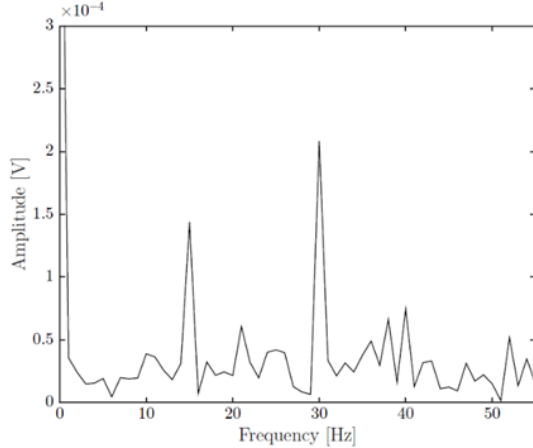


Fig. 13. FFT plot of the sensor output while the pump is operating at 900 RPM.

The two primary peaks identified on the FFT plot correlate to the impeller's rate of rotation. The first peak at 15 Hz is the impeller's rotational frequency and the second peak at 30 Hz is the blade passing frequency. The latter is twice the rotational frequency because the testbed pump uses a two-blade impeller. To measure wear on the impeller blades, the changes in only the peak amplitudes are considered.

To analyze the quality of the output signal collected while the pump is in operation, the signal to noise ratio

$$\text{SNR} = \frac{P_{\text{signal}}}{P_{\text{noise}}} \quad (20)$$

is calculated as the ratio of the signal power  $P_{\text{signal}}$  to the power of the noise  $P_{\text{noise}}$ . To evaluate the sensor SNR, samples are collected at 900 RPM. An interval-dependent Haar wavelet denoising function is applied in MATLAB to separate noise from raw signal. The result is shown in Fig. 14.

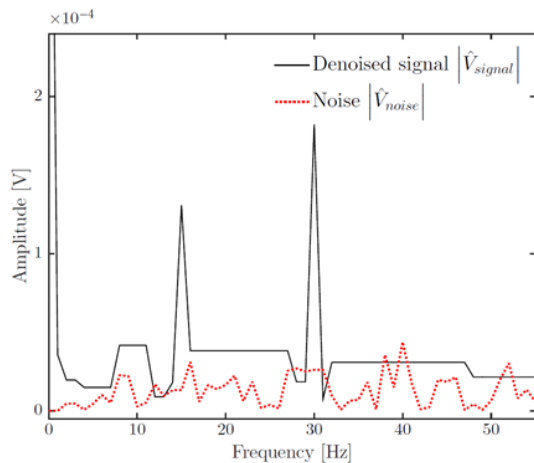


Fig. 14. Output and noise signals at an impeller rotational speed of 900 RPM, sampled at 50 kHz for a duration of 1 second.

The amplitudes at 15 Hz and 30 Hz are the points of measurement interest. Here, the signal to noise ratio is calculated by taking the average between the two resulting values. The SNR at 15 Hz,

$$\text{SNR}_{15} = \frac{\int_{f=13\text{Hz}}^{17\text{Hz}} S_{\text{signal}}(f) \cdot df}{\int_{f=13\text{Hz}}^{17\text{Hz}} S_{\text{noise}}(f) \cdot df}, \quad (21)$$

is measured by integrating the power spectral density of the denoised signal  $S_{\text{signal}}(f)$  and dividing by the integrated power spectral density of the noise signal  $S_{\text{noise}}(f)$  between 13 Hz to 17 Hz. The SNR value at the 15 Hz peak is calculated to be 14.3. The SNR at 30 Hz,

$$\text{SNR}_{30} = \frac{\int_{f=28\text{Hz}}^{32\text{Hz}} S_{\text{signal}}(f) \cdot df}{\int_{f=28\text{Hz}}^{32\text{Hz}} S_{\text{noise}}(f) \cdot df}, \quad (22)$$

is also calculated by integrating the signals from 28 Hz to 32 Hz. This also produces an average SNR value of 14.3. The SNR can also be expressed in decibels,

$$\text{SNR}_{\text{dB}} = 10 \cdot \log_{10} \left( \frac{P_{\text{signal}}}{P_{\text{noise}}} \right), \quad (23)$$

which yields a SNR of 11.6 dB. Increasing the sampling rate an order of magnitude yields a peak SNR of 17.8 dB.

To test the reproducibility of the sensor output, the assembly is completely removed from the pump and placed back again three times while measurements are taken each time the sensor is affixed to the pump. The voltage amplitude at 15 Hz frequency FFT plot for each data set is obtained and the standard deviation between the resulting values is calculated.

Similarly, to quantify the repeatability of the sensor output, 10 sets of one-second measurements are taken from the pump with the same sampling conditions while the sensor is kept affixed to the pump. The standard deviation for both tests is around 10  $\mu\text{V}$  and therefore within an acceptable range; within the noise.

To calibrate the magnetic wear sensor and to observe the change in the output of the sensor as wear accumulates on the tip of the impeller blades of the centrifugal pump, the sensor must take measurements at various stages of the impeller's life while it is being eroded. Since wear occurs very slowly over a period of months or even years, an alternative method for calibrating the sensor is pursued. In this method, the gap between the impeller and the side plate is manually varied to reproduce the effect of wear on the varying gap width inside the pump. To alter the gap, ring gaskets with a thickness of 0.8 mm are inserted behind the pump housing to shift the stuffing box, along with the impeller, outwards. This maintains the gap between impeller and stuffing box while increasing the gap between impeller and side plate, simulating impeller wear. Since the gaskets are slightly compressed when placed inside the pump, the thickness of each gasket is estimated to be  $0.75 \pm 0.05$  mm by measuring the physical change in the

location of the stuffing box with respect to the housing of the pump. The initial clearance inside the pump between the impeller and the side plate is set to  $0.40 \pm 0.05$  mm. Gaskets are then placed one at a time and the process is repeated three times to increase the gap from an initial width of  $0.40 \pm 0.05$  mm to a width of  $2.65 \pm 0.20$  mm. Each time a gasket is inserted, the sensor is installed on the pump and measurements are collected while the pump is running.

The calibration curve for the sensor is shown in Fig. 15. The amplitude of the output signal at 15 Hz is plotted against the magnitude of the varying gap with error bars to describe the uncertainty in the gap width. The standard deviation of the amplitude measurements and are also identified at each gap width. An increased measurement duration results in a reduced standard deviation, leading to a higher accuracy and resolution of the output signal. In steady-state operation, variations in impeller speed were not observed to have a significant effect on measurement accuracy. This is due to the relatively short sampling period and the tendency of the impeller's rotating mass to resist rapid changes in angular velocity.

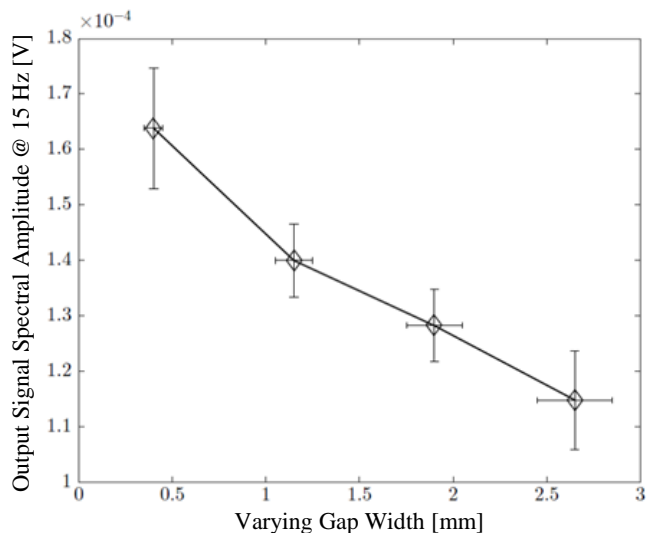


Fig. 15. The spectral amplitude of the sensor's output voltage signal at 15 Hz as a function of impeller gap.

The average sensitivity is determined from the total change in amplitude  $\Delta V$  for the total change in gap width  $\Delta l$  by

$$\bar{S} = \frac{\Delta V}{\Delta l}, \quad (24)$$

which yields 0.022 mV/mm. The resolution achieved by the sensor is

$$\delta l = \frac{\delta V}{\delta \bar{S}}, \quad (25)$$

which is 0.38 mm for an average standard deviation for the amplitude measurement  $\delta V$  of  $8.2 \mu\text{V}$ .

## CONCLUSIONS

This research develops and characterizes a sensor that allows for real-time measurement of impeller wear inside centrifugal pumps. The sensor is a magnetic circuit that passes flux from an inductive coil across the operating pump's impeller. As the impeller erodes over time, the increasing gap is registered as a decrease in inductance of the driving coil, which is converted to a time-dependent output voltage using an auxiliary measurement circuit. When analyzed in the frequency domain, the reduction in peak output voltage is correlated to the extent of impeller wear. The device is portable and adjustable, and can be readily installed on a variety of centrifugal pumps without requiring mechanical modifications or major process disruption.

The sensor demonstrates a signal to noise ratio of 17.8 dB at 500 kHz sampling, with an average sensitivity of 0.022 mV/mm and a gap resolution of 0.38 mm. The achieved sensitivity and resolution make this sensor suitable for impeller wear measurements on a variety of industrial pumps. The standard deviation values for reproducibility and the repeatability of the sensor are both around  $10 \mu\text{V}$ .

The foremost limitation of this sensor is that it requires recalibration for each pump it is placed on. It is also employable for only open-impeller-type centrifugal pumps.

This sensor introduces other opportunities for similar wear or gap measurements inside rotating or non-rotating machinery. For instance, wear measurements on the parallel plates of a pulp refiner could be achieved using this sensor. Clearance or gap measurement inside machinery is also realizable using this sensor, particularly in cases where internal access is limited. However, the fluid in the gap to be measured should be non-magnetic for maximum accuracy and sensitivity.

## REFERENCES

- [1] T. Sahoo and A. Guharoy, "Energy cost savings with centrifugal pumps," *World Pumps*, vol. 2009, no. 510, pp. 35–37, Mar. 2009.
- [2] G. Wood, H. Welna, and R. Lamers, "Tip-clearance effects in centrifugal pumps," *Journal of Fluids Engineering*, vol. 87, no. 4, pp. 932–939, 1965.
- [3] Y. Khalid and S. Sapuan, "Wear analysis of centrifugal slurry pump impellers," *Industrial Lubrication and Tribology*, vol. 59, no. 1, pp. 18–28, Feb. 2007.
- [4] F. Schmaljohann, D. Hagedorn, A. Bu, R. Kumme, and F. Löffler, "Thin-film sensors with small structure size on flat and curved surfaces," *Measurement Science and Technology*, vol. 23, no. 7, p. 074019, Jul. 2012.
- [5] G. Rutelli and D. Cuppini, "Development of wear sensor for tool management system," *Journal of Engineering Materials and Technology*, vol. 110, pp. 59–62, 1988.
- [6] N. Ghosh, Y. Ravi, A. Patra, S. Mukhopadhyay, S. Paul, A. Mohanty, and A. Chattopadhyay, "Estimation of tool wear during CNC milling using neural network-based sensor fusion," *Mechanical Systems and Signal Processing*, vol. 21, no. 1, pp. 466–479, Jan. 2007.
- [7] R. Khoie, "A Magnetic Sensor to Measure Wear in Centrifugal Pumps," M.A.Sc. thesis, Mech. Eng., The University of British Columbia, Vancouver, BC, 2016.
- [8] E. Bohn, "Introduction to Magnetic Fields and Waves," Addison-Wesley Publishing Company, pp. 59 and 170, 1968.
- [9] A. Massarini and M. K. Kazimierczuk, "Self-capacitance of inductors," *IEEE Transactions on Power Electronics*, vol. 12, no. 4, pp. 671–676, Jul. 1997.

- [10] R. Khoie, B. Gopaluni, J. A. Olson and B. Stoeber, "A magnetic sensor to measure wear in centrifugal pumps," 2015 IEEE SENSORS, Busan, pp. 1-4, 2015.